The impact of galaxy colour gradients on cosmic shear measurement

L. M. Voigt,[1]* S. L. Bridle,[1] A. Amara,[2] M. Cropper,[3] T. D. Kitching,[4] R. Massey,[4] J. Rhodes[5,6] and T. Schrabback[7]

[1]*Department of Physics and Astronomy, University College London, Gower Street, London WC1E 6BT*
[2]*Department of Physics, ETH Zürich, Wolfgang-Pauli-Strasse 16, CH-8093 Zürich, Switzerland*
[3]*Mullard Space Science Laboratory, University College London, Holmbury St Mary, Dorking, Surrey RH5 6NT*
[4]*University of Edinburgh, Royal Observatory, Blackford Hill, Edinburgh EH9 3HJ*
[5]*Jet Propulsion Laboratory, California Institute of Technology, 4800 Oak Grove Drive, Pasadena, CA 91109, USA*
[6]*California Institute of Technology, 1201 E California Blvd., Pasadena, CA 91125, USA*
[7]*Kavli Institute for Particle Astrophysics and Cosmology, Stanford University, 382 Via Pueblo Mall, Stanford, CA 94305-4060, USA*

ABSTRACT

Cosmic shear has been identified as the method with the most potential to constrain dark energy. To capitalize on this potential, it is necessary to measure galaxy shapes with great accuracy, which in turn requires a detailed model for the image blurring by the telescope and atmosphere, the point spread function (PSF). In general, the PSF varies with wavelength and therefore the PSF integrated over an observing filter depends on the spectrum of the object. For a typical galaxy the spectrum varies across the galaxy image, thus the PSF depends on the position within the image. We estimate the bias on the shear due to such colour gradients by modelling galaxies using two co-centred, co-elliptical Sérsic profiles, each with a different spectrum. We estimate the effect of ignoring colour gradients and find the shear bias from a single galaxy can be very large depending on the properties of the galaxy. We find that halving the filter width reduces the shear bias by a factor of about 5. We show that, to the first order, tomographic cosmic shear two point statistics depend on the mean shear bias over the galaxy population at a given redshift. For a single broad filter, and averaging over a small galaxy catalogue from Simard et al., we find a mean shear bias which is subdominant to the predicted statistical errors for future cosmic shear surveys. However, the true mean shear bias may exceed the statistical errors, depending on how accurately the catalogue represents the observed distribution of galaxies in the cosmic shear survey. We then investigate the bias on the shear for two-filter imaging and find that the bias is reduced by at least an order of magnitude. Lastly, we find that it is possible to calibrate galaxies for which colour gradients were ignored using two-filter imaging of a fair sample of noisy galaxies, if the galaxy model is known. For a signal-to-noise ratio of 25 the number of galaxies required in each tomographic redshift bin is of the order of 10^4.

Key words: gravitational lensing: weak – cosmology: observations – large scale structure of Universe.

1 INTRODUCTION

Cosmic shear is the weak distortion of distant galaxy images due to the weak gravitational lensing of light by intervening matter. Light rays emitted by galaxies separated by small distances on the sky follow similar paths through the Universe and thus their images are coherently distorted. A statistical analysis of correlations in the cosmic shear signal on different scales therefore provides crucial information about the distribution of dark matter and thus the cosmological model (see e.g. Jarosik et al. 2011). Several upcoming and future observational surveys plan to capitalize on the potential of cosmic shear for discovering the nature of dark energy. These include the ground-based projects the KIlo-Degree Survey (KIDS), Pan-STARRS,[1] Subaru Measurement of Images and Redshifts (SuMIRe),[2] the Dark Energy Survey (DES)[3] and the Large

---

[1] http://pan-starrs.ifa.hawaii.edu
[2] http://sumire.ipmu.jp/en/
[3] http://www.darkenergysurvey.org

*E-mail: lvoigt@star.ucl.ac.uk

Synoptic Survey Telescope (LSST),[4] and the proposed space missions *Euclid*[5] and *WFIRST*.[6]

As surveys become more ambitious and the projected statistical uncertainties on cosmological parameters reduce, the biases associated with shear measurement must be understood and controlled with increasing accuracy. Considerable work has been done on the main systematics, including accurate shear measurement from images (see Heymans et al. 2006; Massey et al. 2007; Bridle et al. 2009, 2010; Kitching et al. 2010, and references therein), requirements on measurement and calibration of galaxy redshifts (Huterer et al. 2006; Ma, Hu & Huterer 2006; Bridle & King 2007; Abdalla et al. 2008; Jouvel et al. 2009; Bernstein & Huterer 2010; Joachimi & Bridle 2010; Zhang, Pen & Bernstein 2010) and methods (see Hildebrandt et al. 2010, and references therein) and accounting for galaxy intrinsic alignments (King & Schneider 2002, 2003; Heymans & Heavens 2003; Heymans et al. 2004; Takada & White 2004; King 2005; Bridle & King 2007; Joachimi & Schneider 2008, 2009; Bernstein 2009; Joachimi & Bridle 2010; Kirk, Bridle & Schneider 2010).

In this paper we consider a crucial aspect of shear measurement: deconvolution of the point spread function (PSF). As light from a galaxy passes through the atmosphere and telescope optics and on to the detector it is convolved with a kernel known as the PSF. The PSF is generally not circular and we typically want to measure cosmic shear for galaxies down to the size of the PSF. The PSF must be accurately determined either from the galaxy spectrum and a detailed model of the telescope or from stars in the image, which can be treated as point objects before the convolution. Several papers have put forward methods for quantifying the spatial (across the detector) and temporal variations in the shape of the PSF (e.g. Jain, Jarvis & Bernstein 2006; Amara, Refregier & Paulin-Henriksson 2010), as well as looking at the number of noisy stars needed to accurately calibrate the PSF model (Paulin-Henriksson et al. 2008; Paulin-Henriksson, Refregier & Amara 2009).

A further issue is the wavelength dependence of the PSF which becomes more important when galaxies are imaged in broad filters. The PSF is a function of wavelength and therefore the observed image consists of the galaxy image at each wavelength, convolved with the PSF at each wavelength, and then integrated over the filter response. Cypriano et al. (2010) investigated the first-order impact of galaxy spectral energy distributions (SEDs) combined with a wavelength-dependent PSF. If the spectrum of the galaxy is not known then in principle this makes it impossible to deconvolve the PSF, even if the PSF shape as a function of wavelength is perfectly known. Cypriano et al. (2010) have shown that the colour information required from ground-based surveys, such as the DES, for estimating galaxy photometric redshifts is enough to provide the required spectral information, if galaxies have the same spectrum at all points on their image.

In this paper we investigate the second order effect of galaxy internal colour gradients (see e.g. Förster Schreiber et al. 2011). This has been highlighted in the context of upcoming space missions (Cypriano et al. 2010), and Hirata & Bernstein (private communication) have shown that, if ignored, the effect can produce shear measurement biases more than an order of magnitude larger than the requirements for upcoming surveys.

Galaxies are often described by two-component models in which the bulge component is redder than the disc component. In this case there is no single PSF across the image if the PSF is a function of wavelength. Using one SED for the bulge component and another for the disc we simulate galaxy images and recover shear values using the PSF for the composite galaxy spectrum across the whole image. The resulting bias is compared to the requirement for future cosmic shear surveys to determine whether a single optical imaging filter is sufficient if galaxy colour gradients are ignored. We use a catalogue of galaxies to find a reasonable range of galaxy parameters. We then repeat the calculation with two filters, allowing estimates of the bulge and disc spectra separately. Finally, we investigate the feasibility of calibrating the bias on a subset of galaxies imaged in more than one filter.

This paper is organized as follows. In Section 2, we describe the galaxy and telescope models used in the simulations. In Section 3, we briefly outline the equations describing the distortion to galaxy images from weak gravitational shear. We then describe in detail the simulations and method used to estimate the biases on the shear and set out the requirements on the bias for future surveys. In Section 4, we quantify the bias on shear estimation from internal colour gradients for single filter imaging. In Section 5, we investigate the improvement gained by imaging in two filters. We then quantify the number of galaxies needed to calibrate the biases in Section 6. Finally we discuss the implications of these results in Section 7.

2 THE GALAXY AND TELESCOPE MODELS

Here we describe the models used to generate the galaxy and PSF images used in the simulations. We also outline the procedure for convolving the sheared multicomponent galaxy images with the PSF.

2.1 The telescope model

The image of a point source is broadened as a result of two dominant wavelength-dependent processes: (1) diffraction giving rise to an Airy disc with size proportional to wavelength and (2) the detector modulation transfer function (MTF) which tends to spread out higher energy photons more than lower energy photons. The PSF intensity map as a function of $\boldsymbol{x}$ for a galaxy with SED $S(\lambda)$ is given by

$$I_{\mathrm{p}}(\boldsymbol{x}) = \frac{\int_0^\infty I_{\mathrm{p}}(\boldsymbol{x}; \lambda) S(\lambda) T(\lambda) \, \mathrm{d}\lambda}{\int_0^\infty S(\lambda) T(\lambda) \, \mathrm{d}\lambda}, \tag{1}$$

where $I_{\mathrm{p}}(\boldsymbol{x}; \lambda)$ is the normalized PSF map at each wavelength, $T(\lambda)$ is the instrumental plus filter response and $\int_0^\infty S(\lambda) T(\lambda) \, \mathrm{d}\lambda$ is the total observed flux from the galaxy.

Throughout the paper we assume a top-hat response function with $T(\lambda) = 1$. For simplicity we model the PSF intensity at each wavelength, $I_{\mathrm{p}}(\boldsymbol{x}; \lambda)$, by a Gaussian with 'half-light radius' (radius enclosing half the total flux) given by

$$r_{\mathrm{p}}(\lambda) = r_{\mathrm{p},0} \left(\frac{\lambda}{\lambda_0} \right)^{0.6}, \tag{2}$$

where $\lambda_0 = 520 \, \mathrm{nm}$ and $r_{\mathrm{p},0} = 0.7$ pixels. The PSF parameters λ_0 and $r_{\mathrm{p},0}$ are chosen so that the full width at half-maximum (FWHM) of the flux-weighted PSF of the fiducial galaxy (see Section 2.4) is approximately 1.7 pixels. The PSF ellipticity and orientation are fixed throughout the paper at $e_{\mathrm{p}} = 0.05$ and $\phi_{\mathrm{p}} = 0°$, respectively. The FWHM and ellipticity of the PSF are chosen to approximately represent the values expected in future cosmic shear surveys.
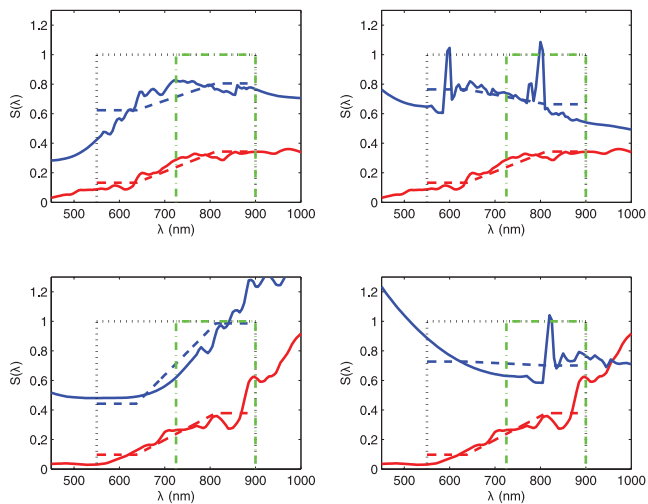

Figure 1. Disc (upper blue solid curves) and bulge (lower red solid curves) for a CWW-Sbc (left-hand panels) and CWW-Im (right-hand panels) disc spectrum for a galaxy at redshift $z = 0.6$ (upper panels) and $z = 1.2$ (lower panels). The bulge spectrum is CWW-E. The response functions $T(\lambda)$ are shown for the F_1 (black dotted) and F_2 (green dash–dotted) filters. The dashed lines show the linear fits to the fluxes in the F_1 and F_2 filters.

We have used an elliptical Gaussian throughout the paper to model the PSF at each wavelength. For more realistic estimates a PSF similar to the instrument in question should be used, for example an Airy disc for a space mission.

The fiducial filters we consider in this paper are a broad top-hat filter with width 550–900 nm, and a narrower filter with width 725–900 nm (hereafter F_1 and F_2, respectively). We choose F_1 to correspond to the filter currently under consideration for the *Euclid* satellite. F_2 is half the linear width of the F_1 filter and at the red end of the F_1 filter. The filter response functions are shown in Fig. 1 along with example bulge and disc galaxy spectra, which are introduced in Section 2.4.

2.2 The galaxy model

In this paper we simulate two-component galaxies with a realistic range of profile shapes and colour gradients. The bulge and disc are modelled by Sérsic profiles (Sersic 1968). The Sérsic intensity at position $\boldsymbol{x} = (x, y)$ is given by

$$I_g(\boldsymbol{x}) = I_0 e^{-k[(\boldsymbol{x}-\boldsymbol{x}_0)^{\mathrm{T}} \boldsymbol{C}(\boldsymbol{x}-\boldsymbol{x}_0)]^{\frac{1}{2n_s}}} \tag{3}$$

where $\boldsymbol{x}_0$ is the centre, I_0 is the peak intensity, n_s is the Sérsic index and $\boldsymbol{C}$ (proportional to the inverse covariance matrix if $n_s = 0.5$) has elements

$$C_{11} = \left(\frac{\cos^2\phi}{a^2} + \frac{\sin^2\phi}{b^2} \right), \tag{4}$$

$$C_{12} = \frac{1}{2} \left(\frac{1}{a^2} - \frac{1}{b^2} \right) \sin(2\phi), \tag{5}$$

$$C_{22} = \left(\frac{\sin^2\phi}{a^2} + \frac{\cos^2\phi}{b^2} \right), \tag{6}$$

where ϕ is the angle (measured anticlockwise) between the x-axis and the major axis of the ellipse and the minor-to-major axis ratio is b/a.

The Sérsic index defines the profile 'type', with $n_s = 0.5$, 1 and 4 for Gaussian, exponential and de Vaucouleurs profiles, respectively. If k is defined as $k = 1.9992 n_s - 0.3271$, then for a circular profile $r_e = a = b$ is the half-light radius. (Note that for a Gaussian profile a^2 and b^2 are the 2D variances if $k = 0.5$; for the circular exponential profile $h = a = b$ is known as the 'scalelength' when $k = 1$.)

The fiducial model used in this paper for the bulge is a de Vaucouleurs profile and for the disc an exponential profile. The FWHM is related to the half-light radius (for a circular profile) via

$$\mathrm{FWHM} = 2r_e \left(\frac{\ln 2}{k} \right)^{n_s}. \tag{7}$$

The total flux (integrated to infinity) emitted by a galaxy described by a Sérsic profile with index n_s is given by

$$F = 2\pi n_s k^{-2n_s} r_e^2 \Gamma(2n_s) I_0, \tag{8}$$

where Γ is the gamma function.

2.3 The galaxy catalogue

The results will depend on the exact assumptions made about the galaxy properties and therefore we use a galaxy catalogue to estimate the average quantities required. The catalogue we use is from a study by Simard et al. (2002) of *Hubble Space Telescope* (*HST*) WFPC2 *F*606*W* (470–720 nm; '*V* band') and *F*814*W* (708–959 nm; '*I* band') observations of the 'Groth Strip'. The catalogue lists galaxy photometric structural parameters obtained from a 2D bulge plus disc decomposition of the galaxy surface brightness profiles. The bulge profile is modelled as a de Vaucouleurs and the disc as an exponential.

Simard et al. (2002) produce two sets of catalogues, one in which fits are performed separately in each filter, and a second catalogue in which the fits are performed simultaneously in each bandpass. We use the second catalogue, which is from the Deep Extragalactic Evolutionary Probe 1 (DEEP1) Keck spectroscopic survey of the Groth Strip (Vogt et al. 2005). The sample is magnitude-limited and contains several objects which were prioritized for selection (see Weiner et al. 2005). The catalogue contains 632 galaxies in the magnitude (Vega) range $(V + I)/2 < 24$ and the median redshift is 0.65.

The catalogue is well-suited to our study because the broad *V* and *I* bands used in the *HST* observations cover a similar wavelength range to the broad F_1 filter. The catalogue provides bulge and disc scale radii (with the bulge scale radius fixed to the same value in each filter, and similarly for the disc scale radius) and the magnitudes of the bulge and the disc in each filter.

We compute linear approximations to the bulge and disc spectra, $S(\lambda)$, across the *V* and *I* bands from the fluxes in each filter using the AB magnitudes given in the catalogue.[7] The bulge SED between the midpoints of the *V* and *I* bands (595–833.5 nm) is given by $S(\lambda) = m_b\lambda + c_b$, where m_b and c_b are the gradient and *y*-intercept of the spectrum, respectively, and similarly for the disc. The spectrum is assumed to be flat between 470–595 nm and 833.5–959 nm, such that $S(\lambda) = m_b\lambda_{V_{\mathrm{mid}}} + c_b$ in the first half of the *V* band and $S(\lambda) = m_b\lambda_{I_{\mathrm{mid}}} + c_b$ in the second half of the *I* band, where $\lambda_{V_{\mathrm{mid}}} = 595$ nm and $\lambda_{I_{\mathrm{mid}}} = 833.5$ nm. The gradient and intercept of the bulge and disc spectra are computed so that the total bulge and disc fluxes in the *V* and *I* bands are equal to the values in the catalogue. If $S(\lambda)$ goes negative in either band then the spectrum is re-set to be flat

---

[7] $m = -2.5 \log_{10}(F) - 48.6$, where m is the AB magnitude and F is the flux.

with a different value on either side of 720 nm, with the constraint that the flux between 470 and 720 nm is equal to the flux in the *V* band, and the flux between 720 and 959 nm is equal to the flux in the *I* band minus the flux between 708 and 720 nm calculated from the flat spectrum between 470 and 720 nm.

The exact distribution of galaxies in a particular survey will depend on the parameters of the survey (e.g. the median redshift), and this must be taken into account when using the results obtained from the catalogue described here to make predictions for future cosmic shear surveys. We investigate the sensitivity of the results to the galaxy redshift and colour distributions in the catalogue in Section 4.2.

We also note that the photometric and structural parameters obtained in the Simard et al. (2002) study will not precisely represent the underlying distribution of galaxy colours and shapes in the DEEP1 survey. This is because (i) the study fits a simple two-component model to the galaxy images, when in fact galaxy morphologies may be complex, and (ii) galaxy images are noisy which may bias the fitted parameters (see Häussler et al. 2007).

2.4 The fiducial galaxy model

We also consider a fiducial galaxy model which is the 'average' galaxy from the catalogue. The fiducial galaxy parameters are $n_{s,b} = 4$, $n_{s,d} = 1$, $r_{e,b}/r_{e,d} = 1.1$, $B/T = 0.25$ and $z = 0.9$. The bulge and disc ellipticities are set equal to $e_b = e_d = e_g = 0.2$. The fiducial values chosen for the ratio of the bulge-to-disc half-light radii and the bulge-to-total flux ratio are the mean values from the catalogue. The central 68 per cent of the $r_{e,b}/r_{e,d}$ distribution is approximately $1.1^{+0.5}_{-0.8}$. The fiducial redshift ($z = 0.9$) is the median value for *Euclid*.

We use a CWW-E spectrum for the bulge throughout the paper, and either a CWW-Sbc or CWW-Im spectrum for the disc (see Coleman, Wu & Weedman 1980). We use the CWW-Sbc spectrum for the fiducial disc spectrum. The spectra observed in the wavelength range 500–1000 nm are shown in Fig. 1 for two different source redshifts. We show in Fig. 2 that these spectra provide a good representation of the distribution of bulge and disc colours found in the catalogue, with the CWW-Sbc spectrum representing the disc $V - I$ colours more closely than the CWW-Im spectrum.

The bulge and disc half-light radii are rescaled (keeping the ratio of the bulge half-light radius to disc half-light radius constant at the fiducial value) throughout the paper so that the ratio of the PSF-convolved galaxy FWHM to PSF FWHM, r_{gp}, is fixed at 1.4 for a circular PSF and galaxy.

2.5 Convolution

The PSF-convolved galaxy intensity at $\boldsymbol{x}$ is given by

$$I_{g*p}(\boldsymbol{x}) = \int_0^\infty I_g(\boldsymbol{x}; \lambda) * I_p(\boldsymbol{x}; \lambda) T(\lambda) \, d\lambda, \quad (9)$$

where $I_g(\boldsymbol{x}; \lambda)$ is the galaxy intensity per unit wavelength. For multiple component galaxies with components i this can be written as

$$I_{g*p}(\boldsymbol{x}) = \sum_i I_{g,i}(\boldsymbol{x}) * I_{p,i}(\boldsymbol{x}), \quad (10)$$

$$I_{p,i}(\boldsymbol{x}) = \frac{\int_0^\infty S_i(\lambda) T(\lambda) I_p(\boldsymbol{x}; \lambda) \, d\lambda}{\int_0^\infty S_i(\lambda) T(\lambda) \, d\lambda}, \quad (11)$$

where $I_{g,i}(\boldsymbol{x})$ is the galaxy intensity integrated over all wavelengths and $S_i(\lambda) T(\lambda) d\lambda$ is the total observed flux from the *i*th component per unit wavelength.

3 QUANTIFYING THE BIAS ON SHEAR MEASUREMENTS

We quantify the bias on cosmic shear measurements from using an incorrect PSF model for a given set of galaxy parameters. We follow Nakajima & Bernstein (2007) and use the 'ring-test' method, described in Section 3.2 (see also Voigt & Bridle 2010). We first briefly outline the equations describing the distortions to galaxy images from gravitational shear before describing the simulations in more detail.

3.1 Gravitational shear

The two-component gravitational shear of a galaxy, given by

$$\gamma = \gamma_1 + i\gamma_2, \quad (12)$$

is related to the projected dimensionless gravitational potential ψ of a thin lens between the source and the observer such that

$$\gamma_1 = \frac{1}{2}(\psi_{11} - \psi_{22}), \quad \gamma_2 = \psi_{12} = \psi_{21}, \quad (13)$$

where $\psi_{ij} = \partial^2 \psi / \partial\theta_i \partial\theta_j$ and $\boldsymbol{\theta}$ is the observed position of the source (see e.g. Bartelmann & Schneider 2001). In the weak lensing regime the reduced shear, g, is approximately equal to the shear γ where
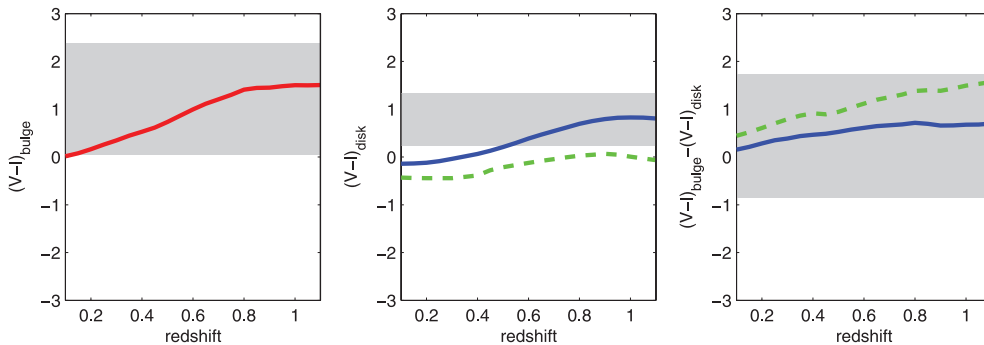
$$g = \gamma/(1 - \kappa), \quad (14)$$

Figure 2. Bulge colour (left), disc colour (middle) and bulge minus disc colour (right) as a function of redshift for a CWW-Sbc (blue solid) and CWW-Im (green dashed) disc spectrum. The bulge spectrum is CWW-E (red solid). Fluxes are measured in the *V* and *I* bands. The shaded regions show the central 68 per cent of the colour distribution measured from galaxies in the catalogue (see Section 2.3).

and the convergence κ is proportional to the projected surface mass density of the lens. A pre-shear elliptical isophote galaxy image with minor-to-major axis ratio b/a and orientation of the major axis anticlockwise from the positive x-axis, ϕ, has a complex ellipticity

$$e^s = \frac{a - b}{a + b} e^{2i\phi}, \tag{15}$$

and is sheared to an ellipse with complex observed ellipticity e^o given by

$$e^o = \frac{e^s + g}{1 + g^* e^s} \tag{16}$$

(Seitz & Schneider 1997) if $\kappa < 1$. We will assume $\kappa \ll 1$ throughout this paper.

3.2 The simulations

We simulate two-component galaxies at different orientations with co-centred, co-elliptical profiles. Each galaxy is sheared by the same amount g using equation (16). The estimated shear for each galaxy is the measured observed ellipticity. We use a ring-test to quantify the bias on the estimated shear for a given galaxy model and PSF estimate in the limit of an infinite number of orientations of the pre-sheared galaxy. For a perfect shear measurement method the average observed ellipticity is then equal to the true input shear. In practice we can reduce the number of galaxies needed in the ring-test by simulating pairs of galaxies separated by 90° (as in Massey et al. 2007). It can be shown from equation (16) that even for a perfect shear measurement method we need at least three pairs of galaxies in the ring-test to reduce the bias on the estimated shear to a negligible level. If the shear measurement method is imperfect (e.g. because the PSF model is incorrect), then we may need more than three pairs to obtain a shear value that has converged to the value we would measure for an infinite number of galaxy orientations. We find, however, that three pairs of galaxies are sufficient to reach convergence. We check that doubling the number of pairs of galaxies does not change the results.

PSF-convolved galaxy images are produced on postage stamps 15^2 pixels in size using the following procedure. The PSF and galaxy models are described in Sections 2.1 and 2.2, respectively. The complex ellipticities of the post-shear bulge and disc are computed using equation (16). The size of each component ($r^2_{e,b}$ and $r^2_{e,d}$) is rescaled by a factor $(1 - |g|^2)^{-1}$ after shearing. The PSF convolutions are performed on a high-resolution image which is 17^2 observational pixels in area and has each observational pixel divided into 7^2 sub-pixels. We find that increasing the number of subpixels used in the convolution beyond 7^2 has a negligible impact on the results. We find that it is necessary to create the galaxy image at an even higher resolution before binning up to make the galaxy image used in the convolution. We find it is sufficient to do this only on the central 5^2 subpixels of the convolution image, but that each of these subpixels must be divided into 25^2 sub-subpixels. The intensity in each subpixel is found by calculating the intensity at the centre of each sub-subpixel and summing all sub-subpixels within each pixel. The intensity in the remaining subpixels of the image is assumed to be equal to the value at the centre of that subpixel. Integration of the intensity within each of the central 5^2 subpixels of the image is necessary for highly peaked profiles, such as the de Vaucouleurs profile used to represent the bulge surface brightness distribution. The convolution with the PSF is performed using fast fourier transforms (FFTs) with sufficient padding such that the result of the convolution is identical to that from performing the convolution

in real space. The high-resolution grid is larger than the postage stamp to allow for light scattered back into the postage stamp due to convolution with the PSF. We check that increasing the resolution parameters does not change the results.

The high-resolution PSF-convolved bulge and disc images are then binned up by a factor of 7 and cut down to produce an image on a postage stamp 15^2 pixels in size. The observed galaxy image is the linear sum of the bulge and disc PSF-convolved images. The bulge and disc are co-centric and co-elliptical and the peak of the intensity profile is within the central pixel of the image grid. The fiducial centre used is $\{x_0, y_0\} = \{0.1, 0.3\}$ pixels relative to the centre of the postage stamp for the galaxy aligned along the x-axis. (In the ring-test the galaxy is rotated around the centre of the grid.) The PSF FWHM is 1.7 pixels and the FWHM of the PSF-convolved galaxy image is 1.4 times the PSF FWHM.

The best-fitting parameters of the bulge and disc components are computed on the image (low-resolution) grid for each angle in the ring-test by minimizing the χ^2 between the true PSF-convolved galaxy image and the PSF-convolved galaxy image using the estimated PSF model. This process is repeated for two different input shears: $\{\gamma^t_1, \gamma^t_2\} = \{0, 0\}$ and $\{\gamma^t_1, \gamma^t_2\} = \{0.01, 0.02\}$, where the superscript 't' refers to the true value of the shear. For each input shear we obtain a shear estimate, $\hat{\gamma}$. We quantify the bias on the shear estimator in terms of multiplicative and additive errors, m_i and c_i, respectively, following Heymans et al. (2006), such that

$$\hat{\gamma}_i = (1 + m_i)\gamma^t_i + c_i, \tag{17}$$

where the subscript i refers to the two shear components and we assume there is no cross-contamination of e.g. $\hat{\gamma}_1$ depending on the value of γ^t_2 or vice versa.

3.3 Survey requirements

We use the requirements on the multiplicative and additive shear biases for cosmic shear two-point statistics computed in Amara & Réfrégier (2008; see also Kitching et al. 2009). These are set so that the systematic error is equal to the statistical error, where the statistical uncertainties depend on the survey area, depth and galaxy number density. For a medium-deep survey of 20 000 deg² (hereafter '*Euclid*-like survey') the upper limits on the total contribution to the multiplicative and additive biases are 10^{-3} and 3×10^{-4}, respectively. Biases a factor of 1–2, 2–5 and 5–20 below the *Euclid*-like survey requirements are shown in the figures by light, medium and dark grey shaded regions, respectively.

The requirements on the shear bias for a particular cosmic shear survey as computed in Amara & Réfrégier (2008) must encompass all systematics involved in the survey (e.g. shear measurement, charge transfer inefficiency or CTE, intrinsic alignments, etc.), and thus to be safe for a *Euclid*-like survey we require the bias from the colour dependence of the PSF to be of the order of a factor of 10 below the upper limits on the multiplicative and additive biases stated above.

4 SINGLE FILTER IMAGING

We calculate shear measurement biases for imaging in a single filter, first considering the dependence of the bias on filter width for some example galaxies, and then calculating the mean bias for single broad-filter imaging by averaging over the catalogue.

4.1 Dependence on filter width and galaxy properties

We first compute the multiplicative and additive biases on the shear for a two-component galaxy imaged in a single visible filter of increasing width with central wavelength 725 nm. For single filter imaging we have no resolved colour information; we assume, however, that the galaxy spectrum from the composite bulge plus disc image is known perfectly from unresolved observations in multiple filters. Such observations are already required for estimating galaxy photometric redshifts. The PSF model is described in Section 2.1. We use the PSF model obtained using the SED from the composite galaxy spectrum (equal to the flux-weighted sum of the true bulge and disc PSF models) for both the bulge and disc PSFs. The galaxy model is described in Section 2.2. The bulge-to-total flux ratio is kept constant as the filter width increases. Variations in the shear bias values are thus dominated by the increase in filter width, and not by a change in the galaxy shape.

The biases are computed using the ring-test method described in Section 3.2. We assume the galaxy model is known. There are seven free parameters in the fits to the single-filter galaxy images: $x_0, y_0, e_g, \phi_g, r_{e,b}, r_{e,d}$ and $I_{0,b}$, where $I_{0,b}$ is the peak intensity of the bulge profile. Note that the peak intensity of the disc profile is known from $r_{e,b}, r_{e,d}, I_{0,b}$ and the total galaxy flux. We assume the total galaxy flux would be obtained from other observations such as the unresolved observations used to obtain the composite spectrum.

Results are shown in Fig. 3 for the fiducial galaxy (red solid lines), as well as for a CWW-Im disc spectrum (black dotted lines) and
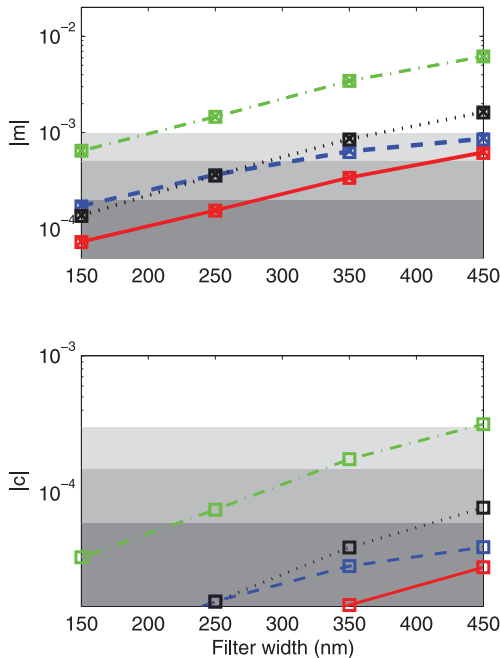
for a different value of the galaxy redshift (blue dashed lines) and $r_{e,b}/r_{e,d}$ ratio (green dot–dashed lines). The shear biases decrease as the filter width decreases because the bulge and disc spectra are in general more similar for smaller widths (and identical for vanishingly small widths). For surveys using broad-band imaging with a filter width of 350 nm (the F_1 filter) the multiplicative biases for the fiducial galaxy considered here are a factor of 3 below the *Euclid*-like survey requirement. The additive bias is a factor of 20 below the requirement. The size of the bias is strongly affected by the ratio of the bulge-to-disc half-light radius, as well as the internal colour gradient, with the multiplicative bias increasing to a factor of $\sim$4 above the requirement and additive bias a factor of $\sim$2 below the requirement for the single departure from fiducial of $r_{e,b}/r_{e,d} = 0.4$. We note that the distribution of bulge-to-disc half-light radii in the galaxy catalogue described in Section 2.3 has mean $r_{e,b}/r_{e,d} = 1.1$, and the central 68 per cent of the distribution is in the range $r_{e,b}/r_{e,d} = 0.3$–1.6.

If we simultaneously make the above multiple departures from the fiducial galaxy the biases are compounded, resulting in a multiplicative bias 30–50 times larger than shown by the red solid curve, depending on the filter width (e.g. for a filter width of 350 nm, $m \sim 10^{-2}$ for $z = 1.4$, $r_{e,b}/r_{e,d} = 0.4$, a CWW-Im disc spectrum and a CWW-E bulge spectrum). For our co-elliptical simulations the multiplicative biases dominate the additive biases and thus we consider only the multiplicative biases in the rest of the paper. We note that for the fiducial galaxy parameters, and keeping the product of the PSF major and minor axes constant, the multiplicative bias increases (decreases) at each filter width by a factor of about 1.5 when the PSF ellipticity is doubled (halved) from the fiducial value of $e_p = 0.05$. The additive bias increases (decreases) at each filter width by a factor of about 3 when the PSF ellipticity is doubled (halved) from the fiducial value.

We now show how different galaxy parameters affect the bias. In Fig. 4 we plot the multiplicative shear biases as a function of bulge Sérsic index, bulge-to-total flux ratio, galaxy ellipticity and position of peak intensity within the central pixel of the postage stamp. We use the same fiducial values as in Fig. 3 with a filter width of 350 nm (F_1 filter). The disc profile is an exponential. The product of the galaxy major and minor axes is kept constant as the galaxy ellipticity is varied. We note there is a dip near $B/T \sim 0.4$ where the bias changes sign. We see that changing the parameters within the ranges shown does not increase the bias above the *Euclid*-like survey requirement. The bias is little affected by the position of the galaxy. However, we see that to determine whether single broad-filter imaging will give biased shear measurements we need to know the true distribution of galaxy shapes and colours in the Universe.

4.2 Averages over the galaxy catalogue

As shown in Section 4.1, the biases on the shear depend on the bulge and disc spectra, the galaxy redshift, the ratio of the bulge-to-disc half-light radii, the bulge-to-total flux ratio, the galaxy ellipticity and the bulge Sérsic index. In this section we compute the biases for single broad-filter imaging with the F_1 filter for a realistic range of galaxy parameters obtained from a catalogue, described in Section 2.3. The catalogue represents an observed range of galaxy colour gradients and bulge-to-disc half-light radii. The bulge Sérsic index is $n_{s,b} = 4$ and we fix the galaxy ellipticity at $e_g = 0.2$ for all galaxies in the catalogue. We see from Fig. 4 that by fixing the bulge Sérsic index and galaxy ellipticity we may over- or underestimate the mean bias by a factor of at most 3, depending on the true distribution of these parameters in the Universe.
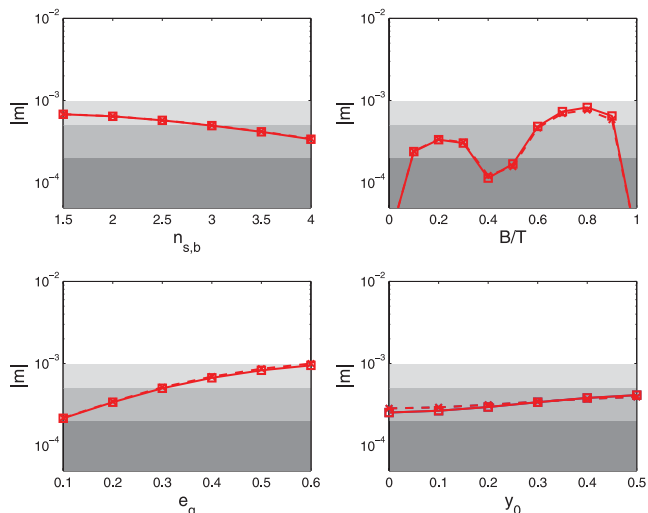

Figure 3. Absolute value of the multiplicative (top) and additive (bottom) shear bias as a function of filter width for imaging in a single filter. The filter transmission function is a top-hat and the central wavelength of the filter is 725 nm. Open squares (crosses) show m_1, c_1 (m_2, c_2). The fiducial galaxy parameters are $z = 0.9$, $r_{e,b}/r_{e,d} = 1.1$, $B/T = 0.25$, a CWW-Sbc disc spectrum and a CWW-E bulge spectrum (red solid). Results are also shown for $z = 1.4$ (blue dashed), $r_{e,b}/r_{e,d} = 0.4$ (green dot–dashed) and a CWW-Im disc spectrum (black dotted), with all other parameters kept at the fiducial values above. Note that c_2 is zero because the PSF is aligned along the x-axis. The shaded regions from light to dark indicate where m_i is a factor of 1–2, 2–5 and 5–20 below the *Euclid* requirement on the bias.

Figure 4. Absolute value of the multiplicative shear bias for imaging in the F_1 filter as a function of the galaxy parameter (clockwise from top left): bulge Sérsic index, bulge-to-total flux ratio, galaxy ellipticity, position of peak intensity relative to the centre of the postage stamp (for the galaxy aligned along the *x*-axis; see Section 3.2; $x_0 = 0.1$). All other galaxy parameters are fixed at the fiducial values (see Section 2.4). The true bulge and disc spectra are CWW-E and CWW-Sbc, respectively. The estimated PSF model for the bulge and the disc components is the model from the composite galaxy spectrum. Solid open squares (dashed crosses) show m_1 (m_2). Shaded regions as in Fig. 3.

For each galaxy in the catalogue we simulate separate 'true' bulge and disc PSF images in the F_1 filter by substituting the linear spectra obtained from the bulge and disc magnitudes (see Section 2.3) into equation (1). Bulge and disc galaxy images are computed and convolved with the PSF images as described in Section 3.2. The bulge and disc shape parameters $r_{e,b}/r_{e,d}$ and B/T are taken from the catalogue. The bulge and disc half-light radii are scaled so that $r_{gp} = 1.4$. In the fits to the 'true' PSF-convolved galaxy images we use the PSF image from the composite galaxy spectrum to estimate both the bulge and disc PSF images. We measure the bias on the shear using a ring-test (as described in Section 3.2) for each galaxy in the catalogue. We assume the galaxy model is known and fit for seven free parameters, described in Section 4.1.

In Fig. 5 we plot the multiplicative biases as a function of the galaxy internal $V - I$ colour gradient (i.e. bulge $V - I$ colour minus disc $V - I$ colour). The bias scales approximately linearly with the colour gradient; the shear is overestimated for negative colour gradients (blue-cored galaxies) and underestimated for positive colour gradients (red-cored galaxies). The mean bias $\langle m_1 \rangle$ over the 632 galaxies in the catalogue is $\sim 3 \times 10^{-4}$, a factor of about 3 below a *Euclid*-like survey requirement, and similar to the value obtained from the fiducial galaxy which was chosen to have average parameters from the catalogue. The bias does not change monotonically with colour gradient because the ratio of bulge-to-disc size is also changing within the catalogue.

We now investigate the sensitivity of the mean bias to the colour distribution of galaxies in the catalogue. In Fig. 6 we plot the mean bias as a function of the percentage of galaxies removed from the catalogue. We investigate the sensitivity to the colour gradient distribution by progressively removing galaxies with the most negative colour gradient, and similarly for the most positive colour gradient (red dashed). The mean bias is equal to the mean bias over the whole
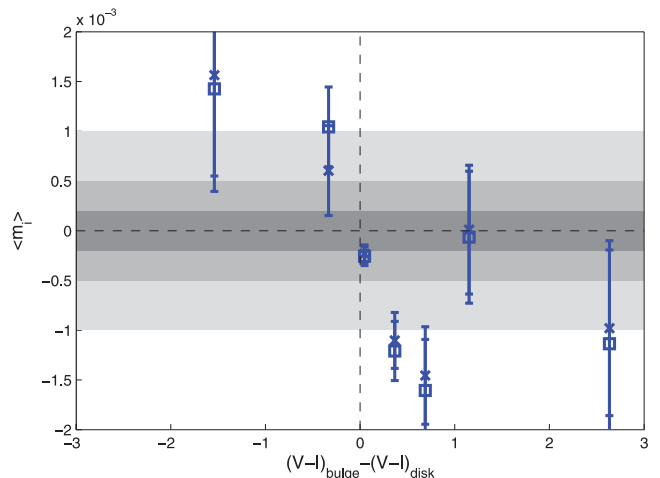

Figure 5. Mean multiplicative bias (m_1 open squares; m_2 crosses) as a function of $V - I$ colour gradient using galaxies from the catalogue (see Section 2.3). Each colour gradient bin contains about 90 galaxies. The galaxy images are simulated in a single broad-filter (F_1) with a top-hat transmission function. The estimated PSF model for the bulge and the disc components is the model from the composite galaxy spectrum. The error bars show the error on the mean bias in each bin (i.e. $\sigma_{m_i}/\sqrt{n_g}$, where σ_{m_i} is the standard deviation of the m_i distribution and n_g the number of galaxies in the bin). Vertical (horizontal) black dashed lines show where the colour gradient ($\langle m_1 \rangle$) is zero. Shaded regions as in Fig. 3.
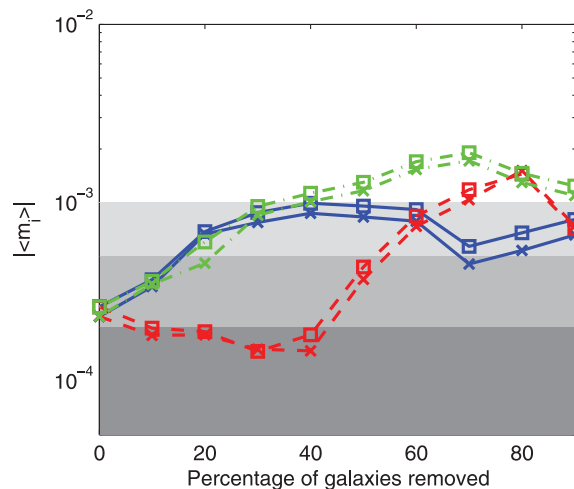

Figure 6. Absolute value of the mean multiplicative bias (m_1 open squares; m_2 crosses) as a function of the percentage of galaxies removed from the catalogue, starting with galaxies with the most negative colour gradient (blue solid), most positive colour gradient (red dashed) and most negative bulge colour (green dot–dashed). Shaded regions as in Fig. 3.

catalogue for 0 per cent removal. If we remove galaxies with the most negative colour gradients (blue-cored galaxies, shown by the blue solid line) then the mean bias increases relative to the mean bias over the complete catalogue by a factor of at most 3. If we progressively remove galaxies with positive colour gradients (red-cored galaxies shown by the red dashed line), then the mean bias initially decreases before increasing to the *Euclid*-like requirement for removal of 60 per cent or more of the catalogue. We note that removing galaxies with the most negative (or most positive) colour gradients increases the mean bias because the distribution of colour gradients in the catalogue is relatively symmetric about zero colour

gradient, and the bias scales approximately linearly with colour gradient.

We also consider the sensitivity of the catalogue to the galaxy redshift distribution. For an *Euclid*-like survey with median redshift $z = 0.9$, the 4000 Å Balmer break is within the F_1 filter, thus we expect to observe a significant fraction of red bulges. We plot the mean bias as a function of the percentage of the 'blue-est' (most negative $V - I$ colour) bulges removed from the catalogue. The mean bias increases to a factor of ~ 2 above the *Euclid*-like requirement for removal of 60 per cent of the blue-est galaxies from the catalogue. Thus if red bulges are under-represented by the catalogue relative to the fraction expected in an *Euclid*-like survey the mean bias for single broad-filter imaging may be close to the systematic error limit of 1×10^{-3}.

As discussed in Section 3.3, the mean bias needs to be a factor of 10 or more below the statistical equals systematic error requirement to be safe for an *Euclid*-like survey, and thus we consider options for reducing the bias below that for single broad-filter imaging. As shown in Section 4.1, the mean bias from single broad-filter imaging may be reduced by imaging in a narrower filter. Alternatively, it may be possible to reduce the mean bias from single broad-filter imaging to the required level by imaging in an additional filter, or by calibrating the bias on a subset of galaxies.

5 TWO-FILTER IMAGING

In this section we investigate how far the biases on the shear may be reduced using two-filter imaging. We repeat the ring-test calculation in Section 4.1 using a narrower filter, F_2 (725–900 nm), in addition to the broad F_1 filter. The narrower filter covers the second half of the wavelength range of the wider filter (see Fig. 1).

The 'true' PSF-convolved galaxy images are generated as described in Section 4.1 using a CWW-E spectrum for the bulge and a CWW-Sbc or CWW-Im for the disc. For two-filter imaging we estimate separate spectra for the bulge and disc components by fitting to the observed two-filter image and using information from the composite galaxy spectrum. We use different PSF models for each of the bulge and disc components ($I_{p,b}^{est}$ and $I_{p,d}^{est}$, respectively), according to their estimated spectra.

We first create linear spectra in which the bulge spectrum is assumed to be flat between $\lambda_{F1,0}$ and $\lambda_{F1,0.25}$ and also from $\lambda_{F1,0.75}$ and $\lambda_{F1,1}$, where $\lambda_{F1,f}$ is the wavelength a linear fraction f across the F_1 filter, for example, $\lambda_{F1,0.25} = 637.5$ nm. Therefore, $S_b(\lambda) = m_b \lambda_{F1,0.25} + c_b$ in the first quarter of the F_1 filter and $S_b(\lambda) = m_b \lambda_{F1,0.75} + c_b$ in the last quarter of the F_1 filter (i.e. the second half of F_2), and similarly for the disc. The gradient and intercept of the bulge and disc spectra are recomputed at each iteration in the fit so that the estimated bulge and disc fluxes in F_1 and F_2 are equal to the integrated fluxes from the linear spectra. If $S_i(\lambda)$ from the linear fits to the fluxes goes negative in either band then the spectrum is reset to be flat with a different value on either side of the midpoint of F_1. Example linear fits to the bulge and disc fluxes are shown in Fig. 1 for redshifts 0.6 and 1.2. In both cases the bulge-to-total flux ratio is 0.25.

Using just the linear spectra fitted to the two filter-resolved images is pessimistic because in reality we would have additional extra unresolved colour information used to produce the composite spectrum. We therefore calculate the residuals between the PSF image obtained using the composite spectrum (equal to the flux-weighted sum of the true bulge and disc PSF images) and the flux-weighted sum of the bulge and disc PSF images obtained from the linear approximations to the spectra ($I_{p,b}^{lin}$ and $I_{p,d}^{lin}$, respectively), equal to

$I_{p,res}$. The residuals are added to the bulge and disc PSF images obtained from the linear approximations to the spectra at each iteration in the fit such that the bulge PSF becomes $I_{p,b}^{est} = I_{p,b}^{lin} + I_{p,res}$, and similarly for the disc.

The bulge PSF is then convolved with the bulge image and the disc PSF with the disc image and the best-fitting galaxy parameters found by minimizing the χ^2 between the sum of these images and the true PSF-convolved galaxy image. There are eight free parameters in the fits, compared with seven free parameters in the single-filter fits. The additional free parameter is the bulge amplitude in F_2. (In practice we fit for the bulge amplitude in F_2 and in the first half of F_1 to ensure that the flux in F_1 is greater than the flux in F_2.) As with the single-filter fits, the disc amplitude in each filter is determined from the bulge flux in the filter and the total flux (assumed known).

The multiplicative biases on the shear for the two-filter configuration are shown as a function of the ratio of the bulge-to-disc half-light radii for different galaxy redshifts in the middle panel of Fig. 7. For comparison the biases for the single broad-filter imaging are shown in the left-hand panel. The right-hand panel is described in Section 6. The central 68 per cent of the $r_{e,b}/r_{e,d}$ distribution from the catalogue ranges from approximately 0.3 to 1.6. The figure shows that the addition of a second narrower filter reduces the biases by more than an order of magnitude. We see that the biases for the two-filter imaging are on average well within the *Euclid*-like survey requirements and thus two-filter imaging on board an *Euclid*-like telescope would be sufficient to correct for the colour dependence of the PSF.

6 BIAS CALIBRATION

In this section we investigate the feasibility of calibrating the biases from internal colour gradients by imaging a subset of galaxies in more than one filter. This subset could be obtained externally, from other existing or dedicated observations by, for example, *HST*, or it could be obtained from within the *Euclid*-like survey itself, which we explore further here. We propose that with real data we would follow the procedure shown in Fig. 9 in which the parameters of each galaxy in the calibration sample are obtained from noisy images of the galaxy observed in two filters. We assume that the galaxy model is known and use the estimated parameters to simulate the galaxy as it would be observed in a single broad filter. Each galaxy is simulated in a ring-test to obtain the shear calibration bias.

We first estimate the number of galaxies required to calibrate the bias from single broad-filter imaging assuming perfect information about the galaxy properties and spectra in the calibration sample (Section 6.1). We then consider in Section 6.2 how well we can estimate the bias from single broad-filter imaging using information from noise-free images of galaxies observed in the F_1 and F_2 filters. Finally, in Section 6.3 we investigate the effects of adding noise to the two-filter images of the calibration data.

6.1 Idealized calibration data

Here we estimate the number of galaxies required to calibrate the bias on cosmic shear measurements from single broad-filter imaging. For a tomographic weak lensing analysis the galaxies will be divided up into 10 or more redshift bins. To correct the bias we need only the mean bias on the shear at each redshift, and not the bias of each individual galaxy (see the appendix).

Consider the optimistic case in which we have perfect information for each galaxy in a calibration sample, for example the spectrum at each point on each galaxy image. This information could be used
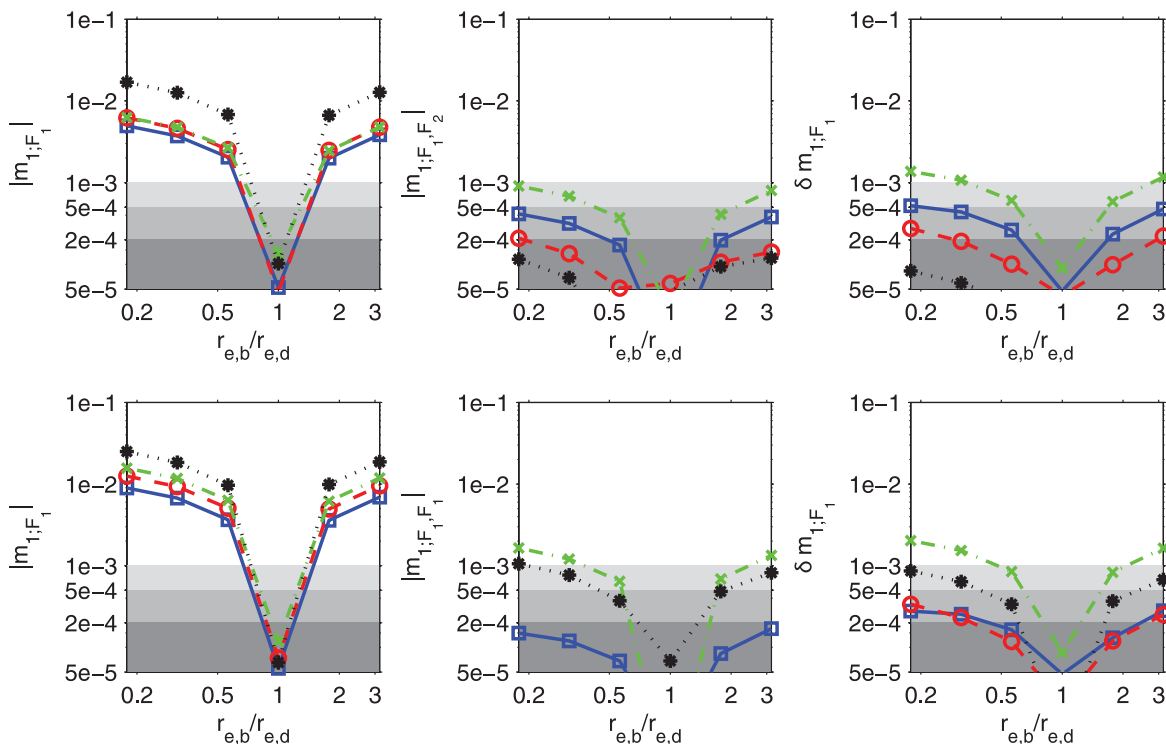
Figure 7. Absolute value of the multiplicative shear bias, $|m_1|$, as a function of the ratio of the bulge-to-disc half-light radii for CWW-Sbc (upper plots) and CWW-Im (lower plots) disc spectra for a galaxy at redshifts 0.4 (blue solid squares), 0.8 (red dashed circles), 1.2 (green dot–dashed crosses) and 1.6 (black dotted stars). Results are shown for imaging in one broad filter (F_1; left-hand plots) and in two filters (F_1, F_2; middle plots). The right-hand plots show the magnitude of the difference between the multiplicative bias obtained by imaging in one filter (F_1) and the estimated bias from imaging in this filter using the bulge and disc shape parameters and spectra obtained from the two filter fits. The bulge-to-total flux ratio is $B/T = 0.25$ and the galaxy ellipticity is $e_g = 0.2$. The bias values for two-filter imaging and a CWW-Im spectrum (lower middle plot) lie below the lower limit on the y-axis for $z = 0.8$. Shaded regions as in Fig. 3.

to estimate the one-filter shear measurement bias for each galaxy in the calibration sample. The average of these numbers could then be used to correct the shear power spectra measured from one-filter imaging of a larger sample. Even though the information on each galaxy is perfect, this could only work if the calibration sample were a fair sample of the Universe, and contained enough galaxies.

We use the distribution of bias values for single broad-filter imaging computed in Section 2.3 from the catalogue to represent the full population of galaxies in a given redshift bin. We draw n_g random samples from the distribution in m to estimate the 1σ uncertainty on the mean multiplicative shear bias for a sample of n_g galaxies. The results are shown as a function of n_g in Fig. 8 as red circles.

We also show the results assuming the distribution in m is Gaussian, so that $\sigma(\langle m \rangle) = \sigma(m)/(n_g - 1)^{0.5}$ (blue line). The results are similar, showing that the distribution in m is well represented by a Gaussian. Therefore, for the optimistic case in which we know for each galaxy in the calibration sample both the galaxy model shape and the spectrum at each point on the galaxy image, we would need 3×10^3 galaxies to calibrate the bias on the shear to a factor of 10 better than the *Euclid*-like survey requirement.

6.2 Two-filter calibration data

We now consider how well the bias from single broad-filter imaging can be calibrated when the galaxies in the calibration sample are
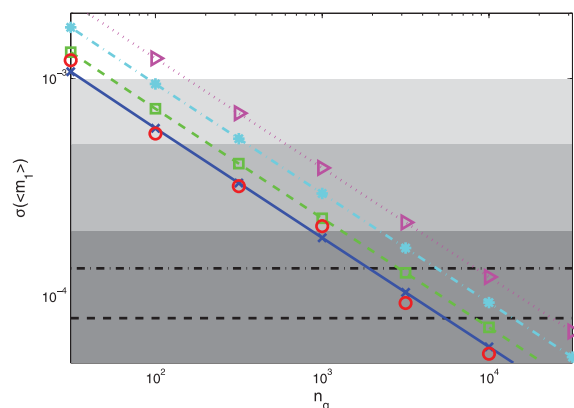

Figure 8. Error on the mean multiplicative bias $m_{1;F_1}$ ($m_{2;F_1}$ omitted for clarity) as a function of the number of galaxies in the calibration sample for a perfect calibration sample and assuming the distribution in $m_{1;F_1}$ obtained using the catalogue is Gaussian (blue crosses solid) and sampling from the true distribution (red circles). Results are also shown for a calibration sample imaged in two filters (F_1 and F_2) with a signal-to-noise ratio of 100 (green squares dashed), 50 (cyan stars dot–dashed) and 25 (magenta triangles dotted) in the F_1 filter. Approximate lower limit on the error on the mean bias for calibration using two-filter imaging assuming a CWW-Sbc (black dashed) and CWW-Im (black dot–dashed) spectrum for the disc. Grey panels as in Fig. 3.
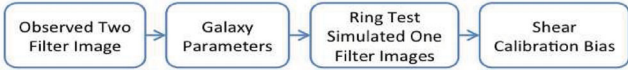
Figure 9. Schematic of our proposal for how to find the one-filter bias from calibration data observed in two filters.

imaged in just two filters. In this case we will not know the bulge and disc spectra precisely, but only linear fits to the bulge and disc fluxes in each filter. There may also be some error on the galaxy shape parameters due to the approximate spectra.

The procedure is outlined in the flow diagram in Fig. 10. We first simulate the 'average' galaxy from the catalogue (see Section 2.4) using a CWW-E spectrum for the bulge and either a CWW-Sbc or CWW-Im spectrum for the disc. We convolve the bulge with the bulge PSF and the disc with the disc PSF (i.e. simulate the true PSF-convolved galaxy image). The shape parameters of the galaxy and linear approximations to the bulge and disc spectra are computed using two-filter imaging in F_1 and F_2 as in Section 5. This is the information that we would obtain for a given galaxy in our calibration sample that could be used to estimate the bias on the shear for single broad-filter imaging. We thus simulate the galaxy using this information and perform a ring-test as in Section 4.1 to obtain an estimate for the bias on the shear when the galaxy is imaged in the F_1 filter only.

We investigate the difference between the true m_{F_1} and m_{F_1} measured from the calibration sample for a range of bulge-to-disc half-light radii and galaxy redshifts. The results are shown in the right-hand panels of Fig. 7 for noise-free galaxy images. The error on m_{F_1} from calibrating in two filters depends on the ratio of the bulge-to-disc half-light radii, the disc spectrum and the galaxy redshift.

We estimate the mean calibration error (i.e. average difference between the true and estimated m_{F_1}) over a population of galaxies. We create a population of galaxies at a given redshift with a CWW-Sbc spectrum for the disc, and the usual CWW-E spectrum for the bulge, and use the ratio of bulge-to-disc sizes from the catalogue. We calculate the error on m_{F_1}, as shown in the right-hand panels of Fig. 7. For practical purposes we restrict our calculation to the range of values in Fig. 7 and if $r_{e,b}/r_{e,d}$ is less than the minimum (maximum) value on the x-axis of the plot then the error is set equal to the value at the minimum (maximum) x-value shown. We repeat the calculation for each of the four redshift values plotted and estimate the mean error on m_{F_1} over redshift by weighting the contribution from galaxies at each redshift using the galaxy redshift distribution from Smail, Ellis & Fitchett (1994): $P(z) \propto z^\alpha \exp[-(1.41z/z_m)^\beta]$, where $\alpha = 2$, $\beta = 1.5$ and the median redshift for an *Euclid*-like survey, $z_m = 0.9$. We repeat the exercise using the CWW-Im spectrum for the disc. The error on m_{F_1} using the CWW-Sbc and CWW-Im spectra is shown by the lower dashed and upper

dot–dashed horizontal lines, respectively, in Fig. 8. The error on the measured bias m_{F_1} cannot be reduced below the values shown by these horizontal lines by increasing the number of galaxies in the calibration sample.

6.3 Noisy two-filter calibration data

We repeat the calculations of the previous section but adding noise to the two-filter simulated images. The noise causes a spread of estimated galaxy parameters and thus increases the width of the distribution of m values and could induce an extra bias.

A broader distribution of m values means that more galaxies will be needed in the calibration sample to measure the mean m_{F_1} to the required accuracy. We add the variance of the m distribution obtained from the catalogue with the variance of the m distribution for the 'average' galaxy from the catalogue whose parameters were obtained from two-filter imaging of noisy images of the galaxy. The number of galaxies required in the calibration sample for different signal-to-noise ratio values is shown in Fig. 8. The signal-to-noise ratio is the value measured in the F_1 filter. We assume the same exposure time in the F_1 and F_2 filters and so the signal-to-noise ratio in F_2 is less than the values quoted. Note for illustration we assume that for a given galaxy the broadening of m_{F_1} due to noise is independent of the galaxy shape parameters and colour gradient and equal to the broadening for the 'average' galaxy.

We check that the mean bias for single-filter imaging in F_1 estimated from two-filter imaging of noisy calibration data is not wrong by more than the requirement on the bias. We find that the difference between the true bias from imaging in a single broad filter and the mean estimated bias over many noise realizations is at least a factor of 2 less than the *Euclid* requirement down to a signal-to-noise ratio of 25. We note that there is no indication that the bias difference increases as the signal-to-noise ratio decreases from 100 to 25.

7 DISCUSSION

To capitalize on gravitational lensing as a cosmological probe it can be attractive to use broad-band imaging to gather as much light as possible and constrain cosmological parameters, including the dark energy equation-of-state parameters, to high precision. Such wide-filter experiments may, however, cause an unacceptable loss in accuracy. In this paper we consider the shear measurement biases arising from single-filter imaging due to the wavelength-dependence of the PSF and the existence of colour gradients across galaxy images.

The PSF is modelled as a Gaussian at each wavelength with ellipticity 0.05. We have assumed a particular wavelength dependence of the PSF size. In practice different telescope designs will have different dependencies depending mainly on the mirror size,
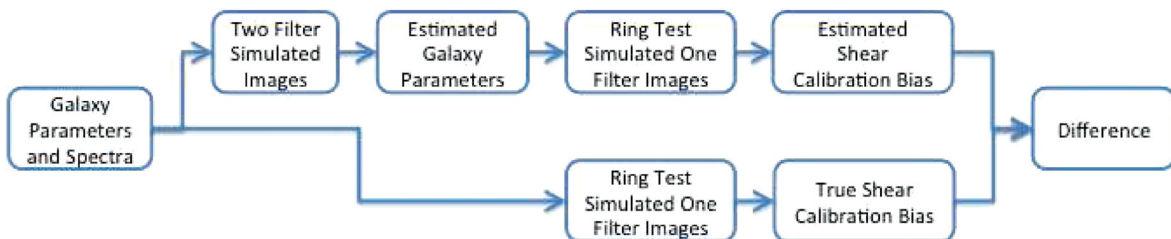

Figure 10. Flowchart to explain how we test whether two filters are sufficient to do the calibration. One-filter shear calibration biases from the estimated galaxy parameters are compared to those from the true galaxy parameters. The estimated galaxy parameters include estimated spectra.

the amount of jitter and the amount of charge diffusion. As can be seen from Cypriano et al. (2010), the optics dominate the PSF wavelength dependence and the biggest likely change would be the relative contribution of the other two (relatively wavelength independent) terms. A decrease in the jitter and/or amount of charge diffusion would increase the wavelength dependence of the PSF. In the worst possible case of zero charge diffusion and no jitter, the slope of the PSF size as a function of wavelength is approximately doubled, which we would naively expect to double the shear measurement biases. In practice the change would be smaller, and if the diffusion or jitter were larger than assumed then the biases would be smaller. We have assumed that the PSF ellipticity is independent of wavelength, but in practice additional components such as beam splitters could introduce wavelength-dependent ellipticity. We assume that the ellipticity, orientation and wavelength dependence of the size of the PSF are all known.

We consider simple bulge plus disc galaxies modelled using two co-centred, co-elliptical Sérsic profiles, each with a different spectrum. The bulge is modelled as a de Vaucouleurs profile and the disc as an exponential. We assume the galaxy model is known and fit for the centre, ellipticity and orientation of the galaxy, the sizes of the bulge and disc components and the bulge-to-total flux ratio. We also assume the composite spectrum emitted by the galaxy is known from ground-based observations and do not take into account errors on the shape of the spectrum or total flux emitted. In practice the different passbands and apertures used from ground and space will make it difficult to obtain the true total flux which will make the estimated biases noisier and potentially biased.

The results will depend on the complexity of the galaxy model. For example, it is possible that non-elliptical isophotes of galaxies can produce non-negligible additive shear calibration biases (Hirata & Bernstein, private communication). However an investigation using more complex models than the elliptical isophote model considered here is beyond the scope of this work. In particular, extending the calculation to more complex galaxy models is non-trivial because current shape measurement methods do not meet the accuracy requirements for an *Euclid*-like survey for realistic signal-to-noise ratio galaxies with radially varying ellipticity isophotes (Bridle et al. 2010), though considerable progress has been made on understanding the limitations of existing methods (Melchior et al. 2010; Voigt & Bridle 2010) and on the development of new methods (Bernstein 2010; Kitching et al. 2010). We note, however, that we obtain similar multiplicative shear biases for high signal-to-noise ratio galaxies to Hirata & Bernstein (private communication). Hirata & Bernstein simulate bulge plus disc galaxies in which the bulge and disc have different ellipticities and use the shape measurement method described in Bernstein (2010). This suggests the results for the multiplicative bias would not change significantly for galaxies simulated with radially varying ellipticity isophotes, provided the shape measurement method used obtains unbiased results on galaxies with no colour gradient.

We first measure the bias on the shear if we ignore colour gradients and image galaxies in a single filter. In the simulations of the 'true' galaxy images we model the bulge spectrum using a CWW-E spectrum and the disc using either a CWW-Sbc or CWW-Im spectrum. We do not take into account evolution of these spectra with redshift as this is much smaller than the difference between the CWW-Sbc and CWW-Im spectra and we show results for both. In the fits to the simulated images we assume the spectrum at each point in the galaxy image is equal to the composite spectrum from the bulge plus disc emission.

We measure the dependence of the bias on the width of the filter for different galaxy parameters. The bias drops by a factor of approximately 5 when the filter width is halved. The bias depends strongly on the galaxy shape parameters as well as on the colour gradient. For a 'typical' galaxy and a filter width of 350 nm the bias is a factor of 3 below the *Euclid*-like survey systematic error limit of 10^{-3}, but the bias can be more than a factor of 10 above the requirement for some galaxy properties considered.

We show that, to the first order, tomographic cosmic shear two-point statistics depend on the mean shear bias over the galaxy population at a given redshift. We compute the mean bias for single broad-filter imaging, averaging over a catalogue of galaxies from a published study of *HST* observations of galaxies in the Keck LRIS DEEP1 survey (Simard et al. 2002). The catalogue is used to represent the range of galaxy colour gradients, shape parameter ratios $r_{e,b}/r_{e,d}$ and bulge-to-total flux ratios in the Universe. We caution, however, that the catalogue has a complicated selection function (see Section 2.3), and that this must be taken into account when drawing conclusions for future cosmic shear surveys. We attempt to investigate the sensitivity of the results to the catalogue by plotting the bias dependence on different galaxy parameters, and by re-computing the mean bias for different colour cuts on the catalogue.

We find that the mean bias over the full catalogue is approximately a factor of 3 below the *Euclid*-like survey requirement. (The mean bias over the catalogue is similar to the bias for the fiducial galaxy because the parameters of the fiducial galaxy are chosen to represent the 'average' galaxy from the catalogue.) However, to ensure the total bias arising from all shear measurement systematics is below the *Euclid*-like requirement, the mean bias from the colour dependence of the PSF should be of the order of a factor of 10 below the systematic equals random error requirement. We thus conclude in Section 4 that single broad-filter imaging in a future *Euclid*-like survey may not allow the accuracy requirements on the bias to be met, depending on how accurately the catalogue from Simard et al. (2002) represents the cosmic shear survey being considered.

We assume that the mean bias obtained using the full catalogue is optimistic because we find it may be up to a factor of 2 larger than 10^{-3} if we modify the galaxy redshift distribution by making colour cuts on the catalogue. However, it is possible that the mean bias computed using galaxy parameter distributions from the catalogue is larger than the true mean bias in an *Euclid*-like survey. This is because the photometric and structural parameters obtained in the Simard et al. (2002) study will not precisely represent the underlying distribution of colours and shapes of galaxies in the DEEP1 survey as a result of fitting a simplified model to noisy galaxies (see Häussler et al. 2007). It is likely that this will result in extreme bulge-to-total flux ratios and colours, increasing the mean bias.

The bias from single broad-filter imaging can be reduced to a negligible level by narrowing the filter; however the survey time or efficiency would have to increase to maintain the same cosmological constraining power. We also consider two other possible options: (i) multiple-filter imaging of the whole survey and (ii) calibrating the bias from single broad-filter imaging on a subset of galaxy images observed in more than one filter. We first investigate how much the biases may be reduced by imaging in two filters. We consider an additional narrower filter with width equal to half the width of the broad filter and fully contained within the broad filter. The colour information available from a two-filter configuration allows us to determine linear approximations to both the bulge and disc

spectra across the broad filter. Using the bulge and disc PSF models calculated from these linear spectra, and including the information from the composite spectrum, the biases are reduced by an order of magnitude below the biases from single broad-filter imaging. Thus, for the simple bulge plus disc galaxy model considered, only one narrow filter is needed in addition to the broad filter to remove the bias from the PSF wavelength dependence to the required accuracy. We note that if the galaxy has more than two components, each with a different spectrum, then two-filter imaging is sufficient to estimate linear approximations to the spectra of each of the components, provided the components are resolved.

We also consider the possibility of calibrating the bias from single broad-filter imaging on a subset of galaxy images. For a tomographic cosmic shear analysis we need the mean multiplicative bias for each redshift bin to be measured to an accuracy of 10^{-4} (i.e. a factor of 10 below the *Euclid* requirement). We note that we expect the mean bias to be redshift-dependent because galaxy morphologies and spectra evolve with redshift. We first compute the number of galaxies needed in the calibration sample to calibrate an *Euclid*-like survey assuming perfect knowledge of the galaxy shape parameters and spectra. Using the distribution of galaxy shapes and colour gradients in the catalogue as a representation of the population of galaxies in the Universe we find that we need approximately 3×10^3 galaxies per redshift bin.

We then investigate whether the information available from noisy two-filter imaging is sufficient to calibrate the bias from single broad-filter imaging. We assume a constant exposure time in the two filters so that the signal-to-noise ratio in the narrower filter is lower than in the broad filter. We find that for a signal-to-noise ratio in the broad filter equal to 25 the number of galaxies required to calibrate the bias in each tomographic redshift bin is of the order of 10^4.

We caution, however, that the calibration strategy assumes the galaxy model is known and further investigation is required to determine whether the procedure will work on low signal-to-noise ratio images of real galaxies with complex morphologies. We check that the error on the calibration bias measured from two-filter imaging of noisy galaxies is sufficiently small down to a signal-to-noise ratio of 25. We do not check lower signal-to-noise ratio values due to computational limitations. We note that in practice it may be possible to stack images with similar properties, e.g. colours, within each redshift bin to reduce the noise.

We have used a simple galaxy model in our proposed calibration strategy because this may capture the main colour gradient effect that causes the shear measurement bias. However this may be insufficiently flexible in practice, depending on the complexity of galaxies in the Universe and any additional shear measurement bias this causes. For this simple galaxy model we find that the shear measurement bias is relatively insensitive to the true galaxy ellipticity (lower left-hand panel of Fig. 4), and therefore galaxies from a calibration sample could be imaged with lower PSF quality than for the main cosmic shear sample. Qualitatively this is because the calibration sample provides information on galaxy colour gradients which has a less stringent image quality requirement than the very stringent requirement for cosmic shear.

We note that the bias value we obtain from the galaxy catalogue cannot be taken to be the true bias for an *Euclid*-like survey because it contains an insufficient number of galaxies and the selection criteria are not matched. The sample contains 632 galaxies over a range of redshifts whereas we conclude that a calibration sample of around 10^4 galaxies per tomographic redshift bin is required. Our conclusions on the number of galaxies needed in a calibration

sample should be more robust though, because the catalogue gives us information about the range of galaxy types in the Universe.

We note that around $r_b = r_d$ the multiplicative bias changes sign. We expect the bias to be zero at $r_b = r_d$ for the simple case where the spectral index of the bulge and disc are the same, because the radial intensity profile would be identical for each component and thus the true PSF-convolved galaxy image equal to the true galaxy image convolved with the PSF for the composite spectrum. We find that when the bulge and disc spectral indices are different the bias is negligible for r_b/r_d close to 1. We note that the average of the Simard catalogue occurs near to this point ($r_b/r_d = 1.1$) and therefore this contributes significantly to the small bias obtained due to the cancellation of large biases of either sign. Again, if the Simard catalogue is atypical then this could lead to a larger bias from realistic data.

ACKNOWLEDGMENTS

REFERENCES

Abdalla F. B., Amara A., Capak P., Cypriano E. S., Lahav O., Rhodes J., 2008, MNRAS, 387, 969
Amara A., Réfrégier A., 2008, MNRAS, 391, 228
Amara A., Refregier A., Paulin-Henriksson S., 2010, MNRAS, 404, 926
Bartelmann M., Schneider P., 2001, Phys. Rep., 340, 291
Bernardeau F., 1998, A&A, 338, 375
Bernstein G. M., 2009, ApJ, 695, 652
Bernstein G. M., 2010, MNRAS, 406, 2793
Bernstein G., Huterer D., 2010, MNRAS, 401, 1399
Bridle S., King L., 2007, New J. Phys., 9, 444
Bridle S. et al., 2009, Ann. Applied Statistics, 3, 6
Bridle S. et al., 2010, MNRAS, 405, 2044
Coleman G. D., Wu C., Weedman D. W., 1980, ApJS, 43, 393
Cypriano E. S., Amara A., Voigt L. M., Bridle S. L., Abdalla F. B., Réfrégier A., Seiffert M., Rhodes J., 2010, MNRAS, 405, 494
Forero-Romero J. E., Blaizot J., Devriendt J., van Waerbeke L., Guiderdoni B., 2007, MNRAS, 379, 1507
Förster Schreiber N. M., Shapley A. E., Erb D. K., Genzel R., Steidel C. C., Bouché N., Cresci G., Davies R., 2011, ApJ, 731, 65
Guzik J., Bernstein G., 2005, Phys. Rev. D, 72, 043503
Hamana T., Colombi S. T., Thion A., Devriendt J. E. G. T., Mellier Y., Bernardeau F., 2002, MNRAS, 330, 365
Häussler B. et al., 2007, ApJS, 172, 615
Heymans C., Heavens A., 2003, MNRAS, 339, 711
Heymans C., Brown M., Heavens A., Meisenheimer K., Taylor A., Wolf C., 2004, MNRAS, 347, 895
Heymans C. et al., 2006, MNRAS, 368, 1323

Hildebrandt H. et al., 2010, A&A, 523, A31
Hirata C. M., Seljak U., 2004, Phys. Rev. D, 70, 063526
Huterer D., Takada M., Bernstein G., Jain B., 2006, MNRAS, 366, 101
Jain B., Jarvis M., Bernstein G., 2006, J. Cosmol. Astropart. Phys., 2, 1
Jarosik N. et al., 2011, ApJS, 192, 14
Joachimi B., Bridle S. L., 2010, A&A, 523, A1
Joachimi B., Schneider P., 2008, A&A, 488, 829
Joachimi B., Schneider P., 2009, A&A, 507, 105
Jouvel S. et al., 2009, A&A, 504, 359
King L. J., 2005, A&A, 441, 47
King L., Schneider P., 2002, A&A, 396, 411
King L. J., Schneider P., 2003, A&A, 398, 23
Kirk D., Bridle S., Schneider M., 2010, MNRAS, 408, 1502
Kitching T. D., Amara A., Abdalla F. B., Joachimi B., Refregier A., 2009, MNRAS, 399, 2107
Kitching T. D. et al., 2010, preprint (arXiv:1009.0779)
Ma Z., Hu W., Huterer D., 2006, ApJ, 636, 21
Massey R. et al., 2007, MNRAS, 376, 13
Melchior P., Böhnert A., Lombardi M., Bartelmann M., 2010, A&A, 510, A75
Nakajima R., Bernstein G., 2007, AJ, 133, 1763
Paulin-Henriksson S., Amara A., Voigt L., Refregier A., Bridle S. L., 2008, A&A, 484, 67
Paulin-Henriksson S., Refregier A., Amara A., 2009, A&A, 500, 647
Seitz C., Schneider P., 1997, A&A, 318, 687
Sersic J. L., 1968, Atlas de galaxias australes. Observ. Astron., Cardoba
Simard L. et al., 2002, ApJS, 142, 1
Smail I., Ellis R. S., Fitchett M. J., 1994, MNRAS, 270, 245
Takada M., White M., 2004, ApJ, 601, L1
Vogt N. P. et al., 2005, ApJS, 159, 41
Voigt L. M., Bridle S. L., 2010, MNRAS, 404, 458
Weiner B. J. et al., 2005, ApJ, 620, 595
Zhang P., Pen U., Bernstein G., 2010, MNRAS, 405, 359

APPENDIX A: IMPACT ON SHEAR POWER SPECTRA OF DENSITY-DEPENDENT SHEAR CALIBRATION

Galaxies with a particular colour gradient will tend to be clustered, for example clusters of galaxies contain a lot of ellipticals which tend to have a small colour gradient, and the converse will be true in voids. In this appendix, we check how this will affect the tomographic lensing power spectrum.

This calculation is related to that by Guzik & Bernstein (2005) who calculate the effect of spatially varying multiplicative shear calibration biases which are uncorrelated with the shear. Here we assume that the multiplicative bias is correlated with the density perturbations and therefore to the shear. There are some parallels between this appendix and calculations of the effect of galaxy number density weighted shear measurements (e.g. see Hirata & Seljak 2004) or source-lens clustering (Bernardeau 1998; Hamana et al. 2002; Forero-Romero et al. 2007), and the shear-intrinsic alignment or gravitational-intrinsic (GI) effect (Hirata & Seljak 2004). However, the former calculations do not consider shear calibration bias.

In this derivation we assume that galaxies have a stochastic multiplicative shear measurement bias m so that the observed shear d is related to the true shear γ by

$$d = (1 + m)\gamma \tag{A1}$$

where m is drawn from a probability distribution whose shape depends on the spatial location $\Pr(m|\boldsymbol{\theta}, z)$. Here we assume that the whole probability distribution is stretched or squeezed uniformly according to the local matter density

$$\Pr(m|\delta) = f((1 + b_{\rm m}\delta)m) \tag{A2}$$

where $b_{\rm m}$ quantifies the sensitivity of the multiplicative bias to the mass distribution. We would expect $b_{\rm m}$ to be negative to obtain the expected reduced multiplicative bias in a local overdensity. Here we choose to assume $b_{\rm m}$ is independent of scale but is an arbitrary function of redshift $b_{\rm m}(z)$, which would depend on galaxy evolution. It would be possible to generalize this derivation for density-independent shear calibration biases discussed in Guzik & Bernstein (2005) by adding in terms to the above equations, but we choose to focus the discussion here on the new effect.

For first order calculations of the shear two-point statistics the relevant property of this distribution will be the mean, $\bar{m}$, which can be written as

$$\bar{m}(\boldsymbol{\theta}, z) = (1 + b_{\rm m}(z)\delta(\boldsymbol{\theta}, z))\bar{\bar{m}}(z), \tag{A3}$$

where $\bar{\bar{m}}$ is the mean multiplicative shear calibration bias averaged over the sky at a given redshift, since $\langle\delta\rangle = 0$. The description of the probability distribution could therefore be more general than described in the paragraph above. Note that to achieve the usual effect of decreased biases at high densities, $b_{\rm m}$ needs to be negative. At very high densities this equation predicts very negative multiplicative shear biases, which would fit with very blue cores in galaxies in the centres of clusters. This is not particularly physical and therefore the model should be improved by using a more sophisticated function of δ which could affect the cancellations in the final result. For example some inverse function of $(1 + \delta)$ could have a more realistic effect at high densities.

The main cosmic shear statistic of interest for future surveys is the tomographic shear power spectrum, which may be defined in terms of the true shear γ

$$C_{\ell ij}^{GG} \equiv \left\langle \left\langle \tilde{\gamma}_{\ell i} \tilde{\gamma}_{\ell j}^* \right\rangle_{\phi\ell} \right\rangle_{\rm r}, \tag{A4}$$

where the inner angle bracket denotes an average over direction of the vector $\boldsymbol{\ell}$ and the outer angle bracket over realizations. We use G to denote true gravitational shear. Here i and j denote the index of the tomographic redshift bins used for the correlation. Tilde denotes the usual Fourier transform in the plane of the sky

$$\tilde{x}_\ell \equiv \int x(\boldsymbol{\theta}) e^{i\boldsymbol{\ell}\cdot\boldsymbol{\theta}}. \tag{A5}$$

The shear γ is related to the mass density δ by the usual equations

$$\gamma(\boldsymbol{\theta}, z) = D(\boldsymbol{\theta}) * \kappa(\boldsymbol{\theta}, z), \tag{A6}$$

where

$$\kappa(\boldsymbol{\theta}, z) = \int {\rm d}z' q(z, z')\delta(\boldsymbol{\theta}, z'), \tag{A7}$$

using the Limber approximation and writing the 3D mass density per unit comoving volume in terms of the position on the sky and redshift. q is the usual lens weight function but the only relevant property of q for this paper is that $q(z, z')$ is zero when $z = z'$.

We assume that tomographic redshift bins are predetermined according to some observable property which is independent of the density field so that the number density of galaxies in redshift bin i as a function of position on the sky and redshift $n_i(\boldsymbol{\theta}, z)$ may be separated out as

$$n_i(\boldsymbol{\theta}, z) = n_i(z)(1 + \delta_{\rm g}(\boldsymbol{\theta}, z)) \tag{A8}$$

where $n_i(z)$ is the mean number density of galaxies at redshift z in redshift bin i averaged over a patch of sky large enough that the mean galaxy density fluctuation $\delta_{\rm g}(\boldsymbol{\theta}, z)$ is zero, normalized such that

$$\int n_i(z)\,{\rm d}z = 1. \tag{A9}$$

We can only calculate statistics of the observed shear d and we here assume this is done by producing a map of d on the sky for each redshift bin. We assume this is done by averaging observed shears in pixels on the sky, therefore this map can be written in the limit of infinite source density as

$$d_i(\boldsymbol{\theta}) = \int \mathrm{d}z \int \mathrm{d}m \ n_i(\boldsymbol{\theta}, z) \Pr(m|\boldsymbol{\theta}, z) \, \mathrm{d}(m, \boldsymbol{\theta}, z) \tag{A10}$$

which can be written to first order in the small quantities as

$$d_i(\boldsymbol{\theta}) = \gamma_i(\boldsymbol{\theta}) + \gamma_{gi}(\boldsymbol{\theta}) + \gamma_{mi}(\boldsymbol{\theta}), \tag{A11}$$

where we have defined

$$\gamma_i(\boldsymbol{\theta}) = \int \mathrm{d}z \ n_i(z)\gamma(\boldsymbol{\theta}, z), \tag{A12}$$

$$\gamma_{gi}(\boldsymbol{\theta}) = \int \mathrm{d}z \ n_i(z)\delta_g(\boldsymbol{\theta}, z)\gamma(\boldsymbol{\theta}, z), \tag{A13}$$

$$\gamma_m(\boldsymbol{\theta}) = \int \mathrm{d}z \ n_i(z) \int \mathrm{d}m \Pr(m|\boldsymbol{\theta}, z)m \, \mathrm{d}m \gamma(\boldsymbol{\theta}, z), \tag{A14}$$

$$= \int \mathrm{d}z \ n_i(z)\bar{m}(\boldsymbol{\theta}, z)\gamma(\boldsymbol{\theta}, z). \tag{A15}$$

We will measure the power spectrum of the observed shear d

$$C_{\ell ij}^{dd} \equiv \left\langle \left\langle \tilde{d}_{\ell i} \tilde{d}_{\ell j}^* \right\rangle_{\phi\ell} \right\rangle_{\mathrm{r}}, \tag{A16}$$

which can be written to first order in the perturbative quantities as

$$C_{\ell ij}^{dd} = C_{\ell ij}^{GG} + C_{\ell ij}^{Gg} + C_{\ell ij}^{Gm} + C_{\ell ij}^{gG} + C_{\ell ij}^{mG}, \tag{A17}$$

where we have defined

$$C_{\ell ij}^{Gg} \equiv \left\langle \left\langle \tilde{\gamma}_{\ell i} \tilde{\gamma}_{g\ell j}^* \right\rangle_{\phi\ell} \right\rangle_{\mathrm{r}}, \tag{A18}$$

$$C_{\ell ij}^{Gm} \equiv \left\langle \left\langle \tilde{\gamma}_{\ell i} \tilde{\gamma}_{m\ell j}^* \right\rangle_{\phi\ell} \right\rangle_{\mathrm{r}}, \tag{A19}$$

where $C_{\ell ij}^{Gg}$ is the same as the term written with the same notation in Joachimi & Bridle (2010), but $C_{\ell ij}^{Gm}$ is different because in this paper we use m to denote the multiplicative shear calibration bias, whereas in that work m was used to denote magnification which we ignore here.

The first term above is the usual shear term and the only one usually considered, the second takes into account the fact that we measure the galaxy number density weighted shear (which contributes to source-lens clustering) and the third term takes into account the possible dependence of the measured shear on a multiplicative shear measurement calibration bias. We write down the source-lens clustering term here because the effect may at first sight seem correlated with the effect discussed in this paper; however from the above equations it can be seen that to the level of approximation considered here the terms are independent, and we thus discuss it no further. Note that the final two terms can be non-zero for overlapping redshift bins.

The cross shear-multiplicative bias term may be further expanded as

$$C_{\ell ij}^{Gm} = C_{\ell ij}^{G\bar{m}} + C_{\ell ij}^{Gmb}, \tag{A20}$$

where we have defined for convenience

$$\gamma_{\bar{m}i}(\boldsymbol{\theta}) = \int \mathrm{d}z \ n_i(z)\bar{m}(z)\gamma(\boldsymbol{\theta}, z), \tag{A21}$$

$$\gamma_{mbi}(\boldsymbol{\theta}) = \int \mathrm{d}z \ n_i(z)\bar{m}(z)b_m(z)\delta(\boldsymbol{\theta}, z)\gamma(\boldsymbol{\theta}, z), \tag{A22}$$

$$C_{\ell ij}^{G\bar{m}} \equiv \left\langle \left\langle \tilde{\gamma}_{\ell i} \tilde{\gamma}_{\bar{m}\ell j}^* \right\rangle_{\phi\ell} \right\rangle_{\mathrm{r}}, \tag{A23}$$

$$C_{\ell ij}^{Gmb} \equiv \left\langle \left\langle \tilde{\gamma}_{\ell i} \tilde{\gamma}_{mb\ell j}^* \right\rangle_{\phi\ell} \right\rangle_{\mathrm{r}}. \tag{A24}$$

We now focus on the second term above and substitute in the relation between shear and mass density. We find

$$\tilde{\gamma}_{\bar{m}\ell i} = \int \mathrm{d}z \ n_i(z)\bar{m}(z)b_m(z) \int \mathrm{d}z' \ q(z', z)A_\ell(z, z'), \tag{A25}$$

where we have defined

$$A_\ell(z, z') = \tilde{\delta}_\ell(z) * \left(\tilde{D}_\ell \tilde{\delta}_\ell(z') \right). \tag{A26}$$

Therefore

$$C_{\ell ij}^{Gmb} = \int \mathrm{d}z \ g_i(z) \int \mathrm{d}z' \ n_j(z')\bar{m}(z')b_m(z') \\ \times \int \mathrm{d}z'' \ q(z'', z')B_{D*\ell}(z, z', z''), , \tag{A27}$$

where we defined

$$B_{D*\ell}(z, z', z'') \equiv \left\langle \left\langle \tilde{D}_\ell \tilde{\delta}_\ell(z) \left(\tilde{\delta}_\ell(z'') * \left(\tilde{D}_\ell \tilde{\delta}_\ell(z') \right) \right)^* \right\rangle_{\phi\ell} \right\rangle_{\mathrm{r}}. \tag{A28}$$

If we assume that mass at one redshift is uncorrelated with mass at another redshift then $B_{D*\ell}(z, z', z''))$ is zero unless $z = z' = z''$. Taken together with the fact that $q(z, z') = 0$ when $z = z'$ it would follow that $C_{\ell ij}^{Gmb} = 0$ at all redshifts. In any case this term depends on the three point function of the mass distribution and is expected to be even smaller than the source-lens clustering term due to the additional factor of $\bar{m}$.

The remaining term $C_{\ell ij}^{G\bar{m}}$ is much simpler and can be written as

$$C_{\ell ij}^{G\bar{m}} = \int \mathrm{d}z \ g_i(z)g_{mj}(z)P(k = \ell/\chi, z), \tag{A29}$$

where we have defined

$$g_{mi}(z) \equiv \int \mathrm{d}z' n_i(z)\bar{m}(z')q(z, z'), \tag{A30}$$

χ is the comoving distance to redshift z and k is the comoving wavenumber. In the special case where $\bar{m}$ is independent of redshift then

$$C_{\ell ij}^{G\bar{m}} = \bar{m} C_{\ell ij}^{GG} \tag{A31}$$

as expected for the simple case where $d = (1 + \bar{m})\gamma$ (note the additional term $C_{\ell ij}^{\bar{m}G}$ which makes up the factor of 2).

Therefore, we have found that the cosmic shear power spectrum is modified to first order by a term proportional to the average of the multiplicative shear calibration bias. In detail there is an additional power spectrum which is identical to the usual lensing power spectrum but in which the lensing weight function is weighted by the mean multiplicative shear calibration bias m at each redshift, spatially averaged over the sky. This is why we require for calibration of this effect the mean multiplicative shear calibration factor at each redshift. This should be spatially averaged rather than galaxy number density averaged. The number of redshift bins in which $\bar{m}$ should be calculated depends on how smoothly it changes with redshift.

This paper has been typeset from a TeX/LaTeX file prepared by the author.